JOURNAL OF AIRCRAFT
Vol. 49, No. 2, March–April 2012

Targeted Parameter Inflation Within Ground-Based Augmentation Systems to Minimize Anomalous Ionospheric Impact

Jiwon Seo*
Yonsei University, Incheon 406-840, Republic of Korea
Jiyun Lee†
Korea Advanced Institute of Science and Technology, Daejeon 305-701, Republic of Korea
and
Sam Pullen,‡ Per Enge,§ and Sigrid Close¶
Stanford University, Stanford, California, 94305

DOI: 10.2514/1.C031601

Anomalous ionospheric conditions can cause large variations in propagation delays of transionospheric radio waves, such as global navigation satellite system (GNSS) signals. Although very rare, extremely large spatial variations pose potential threats to ground-based augmentation system (GBAS) users. Because GBAS provide safety-of-life services, namely precision approach and landing aircraft guidance, system safety must be guaranteed under these unusual conditions. Position-domain geometry-screening algorithms have been previously developed to mitigate anomalous ionospheric threats. These algorithms prevent aircraft from using potentially unsafe GNSS geometries if anomalous ionospheric conditions are present. The simplest ground-based geometry-screening algorithm inflates the broadcast σ_{vig} parameter in GBAS to signal whose geometries should not be used. However, the σ_{vig} parameter is not satellite-specific, and its inflation affects all satellites in view. Hence, it causes a higher than necessary availability penalty. A new targeted parameter inflation algorithm is proposed that minimizes the availability penalty by inflating the satellite-specific broadcast parameters: $\sigma_{pr_{gnd}}$ and P values. In this new algorithm, $\sigma_{pr_{gnd}}$ and P values are inflated by solving optimization problems. The broadcast parameters obtained from this algorithm provide significantly higher availability than optimal σ_{vig} inflation at Newark Liberty International Airport and Memphis International Airport without compromising system safety. It is also demonstrated that the computational burden of this algorithm is low enough for real-time GBAS operations.

I. Introduction

GLOBAL navigation satellite systems (GNSS), such as the Global Positioning System (GPS) in the United States [1,2], the GLONASS in Russia, Compass in China, and the future Galileo in Europe, can be used to support precision approach and landing aircraft guidance. Because the safety requirements of such operations are extremely high, augmentation systems such as ground-based augmentation system (GBAS), also known as the local area augmentation system (LAAS) in the U.S. [3–5], have been developed to augment GNSS for aviation applications. A GBAS ground facility installed at an airport broadcasts differential pseudorange corrections and integrity information to approaching aircraft. When applied by GBAS-equipped aircraft, these differential corrections remove all GNSS errors that are correlated between GBAS ground facility and aircraft receivers. The integrity information warns of unsafe satellites and provides a means for aircraft to reliably bound their position errors to the tiny probabilities required for aviation safety [6].

GNSS signal delay caused by the ionosphere [7–12] is the biggest error source for single-frequency GNSS users, but this error is almost completely mitigated for GBAS-equipped aircraft by applying the broadcast differential pseudorange corrections. This is because ionospheric delay is very highly correlated in space under normal circumstances. Thus, approaching aircraft experience almost the same ionospheric delays as the GBAS ground facility which generates the differential corrections.

However, Datta-Barua et al. [13] first observed very large spatial variations in ionospheric delays of GNSS signals under ionospheric storm conditions. More recently, a maximum ionospheric gradient as high as 413 mm/km [14] has been observed, which is much larger than nominal gradients of 1–4 mm/km [15]. Under severely anomalous ionospheric conditions, signal delays observed by the GBAS ground facility can be very different from the delays observed by an approaching airplane (see Fig. 1). Hence, the ionospheric delay error experienced by an airplane cannot be completely removed by the differential corrections broadcast by the ground facility. Further, the existence of large spatial gradients is not guaranteed to be observed by the code-carrier divergence (CCD) monitor [16] in the GBAS ground facility if the ionospheric pierce point (IPP) between an affected satellite and the ground facility has a similar propagation speed with the ionospheric front (this will be explained further in Sec. II.A). These undetected large ionospheric gradients are potentially hazardous for GBAS-based precision approach guidance.

To meet the system safety (or integrity) requirements for GBAS-based category I precision approach under worst-case anomalous ionospheric conditions, Lee et al. [17,18] proposed the position-domain geometry-screening methodology. Because the CCD and other monitors within the GBAS ground facility cannot detect anomalous ionospheric gradients in a few situations, to guarantee the safety it must be assumed that an undetected large ionospheric gradient always exists with a worst-case geometry, which leads to largest possible range errors. (The current category I GBAS architecture does not incorporate external information regarding ionospheric conditions, such as satellite-based augmentation system or space weather information, although this could change in the future [19].) This method is implemented in the GBAS ground facility and

Received 25 July 2011; revision received 3 October 2011; accepted for publication 3 October 2011.

*Assistant Professor, School of Integrated Technology, 162-1 Songdo-dong, Yeonsu-gu; jiwon.seo@yonsei.ac.kr.
†Assistant Professor, Department of Aerospace Engineering, 335 Gwahangno, Yuseong-gu; jiyunlee@kaist.ac.kr (Corresponding Author).
‡Senior Research Engineer, Department of Aeronautics and Astronautics, 496 Lomita Mall.
§Professor, Department of Aeronautics and Astronautics, 496 Lomita Mall. Member AIAA.
¶Assistant Professor, Department of Aeronautics and Astronautics, 496 Lomita Mall.

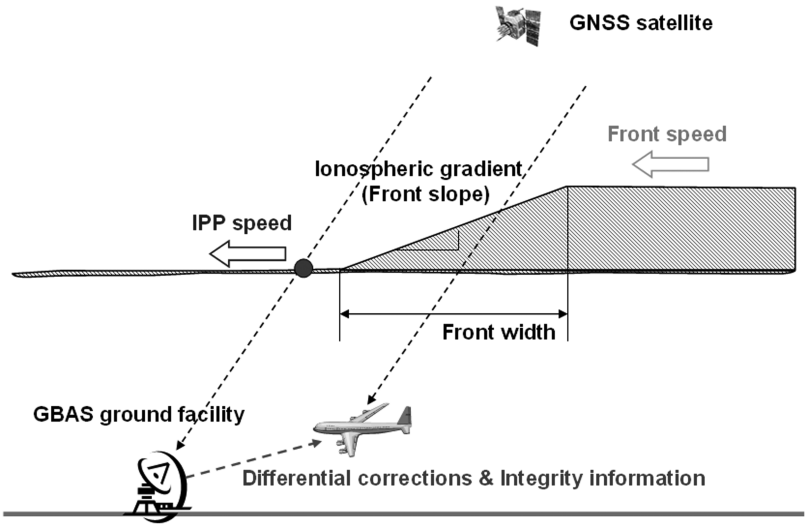

Fig. 1 Potentially hazardous precision approach scenario caused by a very large ionospheric spatial gradient. This large gradient may remain undetected by the CCD monitor of the GBAS ground facility if the IPP speed of the ground facility is almost the same as to the ionospheric front propagation speed. (Reproduction of Fig. 2 of [17].)

requires the ground facility to check each credible satellite geometry (a subset of the set of satellites for which differential corrections are broadcast) that might be used by GBAS-equipped aircraft.

The algorithm calculates the worst possible position errors induced by anomalous ionospheric spatial gradients for all credible satellite geometries. The worst possible position error for a given satellite geometry is a function of the worst possible differential ranging error due to an ionospheric spatial anomaly and the number of satellites that might be affected simultaneously. For category I precision approach operations supported by GBAS in the conterminous U. S. (CONUS), a threat model defining these parameters has been developed based upon validated observations of severe ionospheric spatial gradients observed in CONUS since 1999 [14,15].

To meet the GBAS safety requirements, credible subset satellite geometries with worst possible position errors larger than a separately-defined tolerable error limit (TEL) must not be used by GBAS-equipped aircraft. To make aircraft screen out those unsafe subset geometries, one or more of the integrity parameters broadcast by GBAS are inflated to increase the position error bounds of unsafe geometries over the category I alert limit so that they cannot be approved for use by GBAS avionics (see Sec. II.B for details) [17]. Geometry screening via inflating the broadcast σ_{vig} parameter, as implemented in [17], guarantees system safety as long as the chosen threat model properly bounds worst-case ionospheric behavior. A variant of this algorithm has been adopted by the Honeywell SLS-4000 category I LAAS ground facility intended for operational use [20].

Although geometry screening protects system integrity, it has the inevitable side effect that system availability is reduced (meaning that fewer satellite geometries can be used for category I operations) because it increases the position error bounds of all geometries, including the vast majority that are safe even in the presence of the worst-case ionospheric anomaly. Because the current GBAS ground facility does not have access to external information that would allow it to reliably differentiate between nominal and anomalous ionospheric conditions, it must protect against worst-case anomalous conditions at all times. This resulting loss of availability is particularly prominent in σ_{vig} inflation because the σ_{vig} parameter is not satellite-specific; thus, a single inflated value affects all satellites in view.

To overcome this limitation, Ramakrishnan et al. [21] proposed to inflate two satellite-specific parameters, $\sigma_{pr_{\text{gnd}}}$ and P values, to reduce unnecessary increases in position error bounds. Unlike σ_{vig} inflation, where only one selectable parameter exits, $2N$ optimization parameters exist in this case (N $\sigma_{pr_{\text{gnd}}}$ values and N P values, where N is the number of satellites in view). Because the inflation algorithm must support real-time operations, its computational cost is critical. For this reason, a heuristic and computationally efficient way to inflate $\sigma_{pr_{\text{gnd}}}$ and P values was proposed in [21] without specific optimization criteria.

We adopt the idea of targeted inflation of the same satellite-specific parameters in this paper, but we propose a novel way to obtain those parameters by formulating and solving optimization problems instead of relying on heuristics (Sec. III). The resulting nonlinear optimization problems may not be solvable in real time. Hence, we simplify them to linear programming (LP) problems. The availability benefit of this algorithm, which does not compromise system integrity, is demonstrated at Newark Liberty International Airport and Memphis International Airport (Sec. IV.A). Its computational efficiency and other practical considerations are discussed in Sec. IV.B. Our conclusions are given in Sec. V.

II. Ionospheric Threats on GBAS and Mitigation by Position-Domain Geometry Screening

This section further examines potential integrity threats to GBAS caused by anomalous ionosphere. In addition, the σ_{vig}-based position-domain geometry-screening algorithm that was proposed in [17,18] and implemented by the Honeywell SLS-400 category I LAAS ground facility [20] is briefly reviewed in this section.

A. Ionospheric Threats to Category I GBAS Operations

As described in Sec. I, given worst-case airplane and ionospheric front movement geometries, a large ionospheric gradient may be unobservable to the GBAS ground facility. Undetected and hence unmitigated ionosphere-induced errors can pose integrity threats to a GBAS-guided airplane.

Figure 2 shows the details of a potentially hazardous ionospheric scenario based on the threat model developed for category I GBAS in CONUS. The points in this figure show the IPPs of all satellites in view of a GBAS ground facility at a given time. An IPP represents a theoretical point in space where the line of sight between a receiver and a satellite intersects an imaginary thin shell at a selected altitude in the ionosphere where all of the signal delay caused by the ionosphere is assumed to occur (a thin-shell height of 350 km is assumed in this paper).

While an airplane is approaching a runway, an ionospheric front can impact two IPPs simultaneously. The CCD monitor in the GBAS ground facility detects the time-variation of divergence between code and carrier measurements. If an IPP velocity projected to an ionospheric front direction ($V_{k1,\text{proj}}$ in Fig. 2) is very close to an ionospheric front velocity (V_{front}), their relative speed ($\Delta v_{k1} = |V_{k1,\text{proj}} - V_{\text{front}}|$) is close to zero. Thus, a significant level of

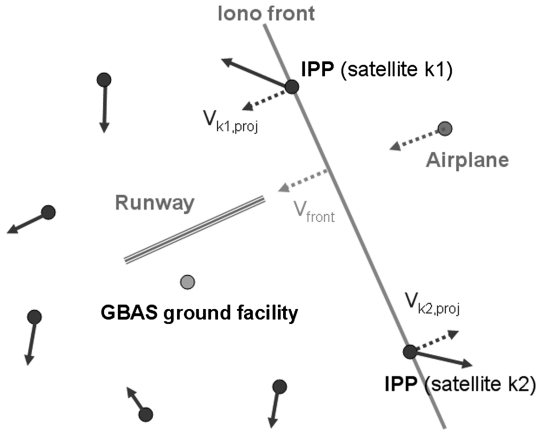

Fig. 2 Worst-case geometry of ionospheric front and ionospheric pierce points under two-satellite impact scenario. Because the ionospheric front speed (V_{front}) is the same as the projected IPP speed of satellite $k1$ ($V_{k1,\text{proj}}$), the large ionospheric gradient impacting satellite $k1$ is unobservable by the CCD monitor in the GBAS ground facility. However, the CCD monitor has a much higher chance to detect the ionospheric gradient impacting satellite $k2$.

time-varying divergence would not be observed by the CCD monitor in this scenario, meaning that the ground-based CCD monitor could not detect the existence of a large ionospheric gradient impacting satellite $k1$. Hence, to guarantee safety, an anomalous ionospheric gradient must be assumed to exist even though no evidence of this anomaly appears in the outputs of the CCD monitor (or other ground-system monitors). Furthermore, the magnitude of a hypothetical undetected ionospheric gradient must be the largest possible value in the ionospheric threat model (e.g., [14,22]) for the corresponding geographical region.

On the other hand, there typically exists a significant relative speed for satellite $k2$ ($\Delta v_{k2} = |\mathrm{V}_{k2,\text{proj}} - \mathrm{V}_{\text{front}}|$) if V_{front} is assumed to be equal to (or very similar to) $V_{k1,\text{proj}}$ in the two-satellite impact scenario in Fig. 2. Because of this large Δv_{k2}, the ionospheric gradient impacting satellite $k2$ is usually detectable, and ionosphere-induced differential range errors for satellite $k2$ do not increase as much as the worst case experienced on satellite $k1$. (Although the gradient impacting satellite $k2$ is detectable, differential range errors for satellite $k2$ would increase up to certain amounts depending on Δv_{k2} before actual detection.) Based on a mathematical model of the CCD monitor, closed-form expressions of an ionosphere-induced differential range error ε depending on the magnitude of the relative speed Δv under the CONUS threat model are given in [17,21,23].

$$\varepsilon = \min\left(\frac{50}{w}, g\right) \times (x_{\text{aircraft}} + 2\tau v_{\text{aircraft}}),$$
$$\text{if } \Delta v < \frac{0.0229}{\min(\frac{50}{w}, g)} \quad \text{and} \quad \Delta v < 0.11$$

$$\varepsilon = 4, \qquad \text{if } \frac{0.0229}{\min(\frac{50}{w}, g)} < \Delta v < 0.11$$

$$\varepsilon = 2.5, \qquad \text{if } \Delta v > 0.11$$

where ε is ionosphere-induced differential range error in meters; w is the ionospheric front width in kilometers; g is the ionospheric gradient in meters per kilometer; x_{aircraft} is the physical separation between the GBAS ground facility and an approaching airplane in kilometers; τ is the time constant of the single-frequency GBAS carrier smoothing filter (100 s for category I GBAS); v_{aircraft} is the velocity of an approaching airplane in kilometers per second (a constant velocity of 0.07 km/s is assumed in this paper); and Δv is the relative speed between the ionospheric front velocity and the projected velocity of an IPP in kilometers per second.

Once ionosphere-induced differential range errors ε_{k1} and ε_{k2} are obtained for a given two-satellite impact scenario, an ionosphere-induced error in vertical (IEV) can be calculated using Eq. (1) or Eq. (2). IEV represents a worst possible vertical position error due to a worst observed ionospheric gradient impacting a given satellite pair with worst-case geometry, as shown in Fig. 2. Although Eq. (1) provides a theoretical maximum IEV value that has been widely adopted (e.g., [23,24]), Lee et al. [17] have recently shown that Eq. (1) is unnecessarily conservative. They proposed Eq. (2) as a more general expression for IEV calculation and showed that Eq. (1) is an extreme case of Eq. (2) when the c factor in Eq. (2) is equal to 1 (see appendix of [17] for proof). Considering all anomalous ionospheric gradients observed in CONUS, including a dual-front scenario, $c = 0.5$ was suggested as a very conservative bound (see [17] for details).

$$\text{IEV}_{k1,k2} = |S_{\text{vert},k1}\varepsilon_{k1}| + |S_{\text{vert},k2}\varepsilon_{k2}| \tag{1}$$

$$\begin{aligned}\text{IEV}_{k1,k2} = \max\{&|S_{\text{vert},k1}\varepsilon_{k1} + S_{\text{vert},k2}\varepsilon_{k2}|, |S_{\text{vert},k1}\varepsilon_{k1} \\ &- c \cdot S_{\text{vert},k2}\varepsilon_{k2}|, |S_{\text{vert},k2}\varepsilon_{k2} - c \cdot S_{\text{vert},k1}\varepsilon_{k1}|\}\end{aligned} \tag{2}$$

$$\begin{aligned}&S \equiv (G^T W G)^{-1} G^T W \\ &G_i = [\,-\cos El_i \cos Az_i \quad -\cos El_i \sin Az_i \quad -\sin El_i \quad 1\,] \\ &W^{-1} = \begin{bmatrix} \sigma_1^2 & 0 & \cdots & 0 \\ 0 & \sigma_1^2 & \cdots & 0 \\ \vdots & \vdots & \ddots & \vdots \\ 0 & 0 & \cdots & \sigma_N^2 \end{bmatrix}\end{aligned} \tag{3}$$

where $S_{\text{vert},ki}$ is the vertical position component of the weighted-least-squares projection matrix S for satellite ki (refer to Section 2.3.10.2 in [6]) and is dependent on the satellite geometry (the number and geometric distribution of satellites in view) at each epoch; ε_{ki} is the ionosphere-induced range error for satellite ki; c is a dimensionless constant between 0 and 1 ($c = 0.5$ was suggested as a very conservative bound on any observed ionospheric conditions in CONUS [17]); G_i is the ith row of the observation matrix G, corresponding to the ith satellite in view (satellite i, for simplicity); El_i is the elevation of satellite i; Az_i is the azimuth of satellite i; W^{-1} is the inverse of the least-squares weighting matrix; and σ_i^2 is the variance of a normal distribution that overbounds the true post-correction range-domain error distribution for satellite i under the fault-free hypothesis.

Satellite locations and velocities at each epoch are known to acceptable accuracy from the broadcast GPS almanacs, and the two-satellite impact scenario in Fig. 2 can be assumed for all satellite pairs. (As discussed in [17], three or more satellite impact scenarios of the pattern shown in Fig. 2 are extremely improbable, and they are generally no more threatening than the worst two-satellite impact case.)

Each satellite pair has one worst-case IEV, and the maximum (worst case) over all IEVs for all satellite pairs of a given subset satellite geometry at a given epoch is called maximum IEV (MIEV). If an MIEV is larger than the TEL in the vertical direction derived from the category I obstacle clearance surface [25], the satellite geometry in question is not acceptable for GBAS-based category I precision approach; thus, the unsafe geometry must not be approved for use by aircraft using GBAS.

Figure 2 shows an example satellite geometry of the GBAS ground facility. In most cases, an approaching airplane has the same satellites in view as the ground facility. However, an airplane may occasionally lose one or two satellites while maneuvering or during conditions where tracking is impaired. Thus, it is usually assumed that up to two satellites in view of the GBAS ground facility may not be usable by an approaching airplane. In this case, the number of independent subset satellite geometries that could be used by aircraft is

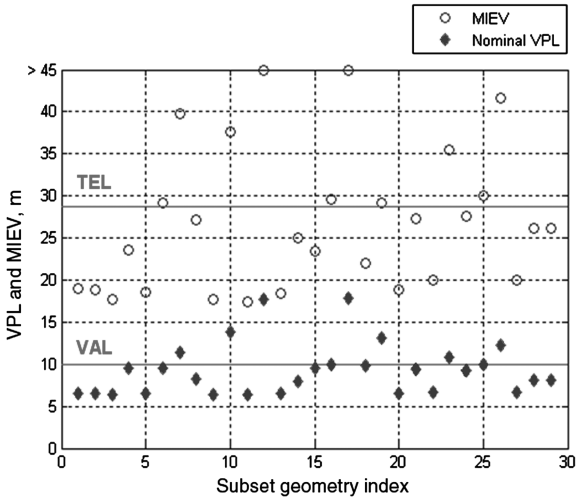

Fig. 3 MIEVs and VPLs at a certain epoch at Newark Liberty International Airport. The geometries with VPLs exceeding VAL are not approved by airborne GBAS receivers. Thus, they are not hazardous, even though their MIEVs are larger than TEL.

$$\sum_{k=N-2}^{N}\binom{N}{k}$$

where N is the number of satellites for which differential corrections are broadcast by the ground facility. Because any of these subset geometries can be used by aircraft, a separate MIEV should be calculated for each of them. If an MIEV of a particular subset geometry exceeds TEL, the subset geometry must not be approved for precision approach.

Figure 3 shows an example of MIEVs at a certain epoch at Newark Liberty International Airport. There are seven satellites in view at this epoch; as is normally the case, all are presumed to be healthy and thus have differential corrections broadcast by the GBAS facility at Newark. Thus,

$$\sum_{k=5}^{7}\binom{7}{k} = 29$$

subset satellite geometries are potentially visible to aircraft. The geometry index 1 in Fig. 3 represents the all-in-view satellite geometry, and the other indices have no particular order. In this example, the subset geometries with MIEVs exceeding TEL (i.e., geometries 6, 7, 10, 12, 16, 17, 19, 23, 25, and 26) are potentially hazardous for category I precision approach, and they must not be approved to use by aircraft. (TEL is 28.78 m at the minimum decision height of 200 ft for category I precision approach [25].)

Airborne GBAS receivers calculate the confidence bounds of their position solutions at each epoch. The vertical confidence bound is called the vertical protection level (VPL), which is obtained from Eqs. (4) and (5). If either VPL_{H0} or $\mathrm{VPL}_{\mathrm{eph}}$ is greater than the vertical alert limit (VAL) of the desired operation, the operation is not approved by a GBAS receiver. As an example, the VPL of each subset geometry is also plotted in Fig. 3. These VPLs are simulated with nominal broadcast parameters of the GBAS ground facility. Each VPL value in Fig. 3 is the larger of VPL_{H0} and $\mathrm{VPL}_{\mathrm{eph}}$. For geometries 7, 10, 12, 17, 19, 23, and 26, VPLs are greater than the 10 m VAL for category I precision approach at the 200 ft decision height [6]. Hence, those geometries are not approved for precision approach. By this VPL calculation and VAL comparison, some potentially hazardous geometries with MIEVs exceeding TEL (i.e., geometries 7, 10, 12, 17, 19, 23, and 26) are removed from the approved set of geometries. Thus, those geometries cannot be hazardous, regardless of MIEV, because they will not be approved by GBAS receivers. However, other geometries with MIEVs exceeding TEL (i.e., geometries 6, 16, and 25) are still unsafe to use because their VPLs are lower than the VAL; thus, they would be approved by a receiver if nothing else were done. To remove these unsafe geometries from an approved set of geometries, position-domain geometry screening has been proposed [17,18] and will be reviewed in the following subsection.

$$\mathrm{VPL}_{H0} = K_{\mathrm{ffmd}}\sqrt{\sum_{i=1}^{N} S_{\mathrm{vert},i}^2\sigma_i^2} \tag{4}$$

$$\mathrm{VPL}_{\mathrm{eph}} = \max_k(\mathrm{VPL}_{\mathrm{eph},k}) \quad \text{and}$$

$$\mathrm{VPL}_{\mathrm{eph},k} = |S_{\mathrm{vert},k}|x_{\mathrm{aircraft}}P_k + K_{md_{\mathrm{eph}}}\sqrt{\sum_{i=1}^{N} S_{\mathrm{vert},i}^2\sigma_i^2} \tag{5}$$

where VPL_{H0} is the VPL (bound on vertical position error) under the fault-free hypothesis; K_{ffmd} is a multiplier (unitless) that determines the probability of fault-free missed detection ($K_{\mathrm{ffmd}} = 5.847$ for four ground subsystem reference antennas is used here; refer to Section 2.3.11.5.2.1.4 in [6]); $S_{\mathrm{vert},i}$ is the vertical position component of the weighted-least-squares projection matrix for satellite i; σ_i^2 is the variance of a zero-mean Gaussian distribution that overbounds the true range-domain post-correction error distribution for satellite i under the fault-free hypothesis; $\mathrm{VPL}_{\mathrm{eph},k}$ is the VPL under a single-satellite (satellite k) ephemeris fault; x_{aircraft} is the physical separation between the GBAS ground facility and the approaching airplane; P_k is the ephemeris error decorrelation parameter for satellite k (also known as P value); and $K_{md_{\mathrm{eph}}}$ is a multiplier (unitless) derived from the probability of missed detection given that there is an ephemeris error in a GNSS satellite ($K_{md_{\mathrm{eph}}} = 5.085$ is used in this work; refer to [23,24]).

B. Position-Domain Geometry Screening by σ_{vig} Inflation

The first part of position-domain geometry screening is to calculate the MIEVs of all potentially-usable subset satellite geometries, as explained in the previous subsection. Some unsafe subset geometries are not screened out by the airborne receiver VPL calculation and VAL comparison based upon the nominal broadcast parameters from the GBAS ground facility. When this is the case, geometry screening acts to inflate receiver VPLs over VAL until all unsafe geometries are screened out. To inflate VPL without any modifications to airborne GBAS receivers or communication protocols, the GBAS ground facility needs to increase or inflate one or more of its broadcast parameters that affect VPL. By inflating the σ_{vig} parameter in Eq. (8), σ_i^2 in Eq. (6) and thus VPL_{H0} and $\mathrm{VPL}_{\mathrm{eph}}$ in Eqs. (4) and (5) naturally increase as functions of the ground facility to aircraft separation distance x_{aircraft}. Hence, the σ_{vig} parameter is a good candidate for inflation.

$$\sigma_i^2 = \sigma_{pr_{\mathrm{gnd}},i}^2 + \sigma_{\mathrm{tropo},i}^2 + \sigma_{pr_{\mathrm{air}},i}^2 + \sigma_{\mathrm{iono},i}^2 \tag{6}$$

$$\sigma_{pr_{\mathrm{air}},i}^2 = \sigma_{\mathrm{multipath},i}^2 + \sigma_{\mathrm{noise},i}^2 \tag{7}$$

$$\sigma_{\mathrm{iono},i} = F_i\sigma_{\mathrm{vig}}(x_{\mathrm{aircraft}} + 2\tau v_{\mathrm{aircraft}}) \tag{8}$$

where σ_i^2 is the variance of a normal distribution that overbounds the true post-correction range-domain error distribution for satellite i under the fault-free hypothesis (this paper uses the same error models used in [17,23,24]); $\sigma_{pr_{\mathrm{gnd}},i}$ is the total fault-free one-sigma ground error term associated with the corresponding differential correction error for satellite i; $\sigma_{\mathrm{tropo},i}$ is the one-sigma ground error term associated with residual tropospheric uncertainty for satellite i; $\sigma_{pr_{\mathrm{air}},i}$ is the one-sigma error term that bounds fault-free airborne receiver measurement error for satellite i; $\sigma_{\mathrm{multipath},i}$ is the fault-free one-sigma airborne error term associated with multipath error for satellite i; $\sigma_{\mathrm{noise},i}$ is the fault-free one-sigma airborne error term associated with receiver noise for satellite i; $\sigma_{\mathrm{iono},i}$ is the one-sigma ground error term associated with residual ionospheric uncertainty for satellite i; F_i is

the vertical-to-slant ionospheric thin shell model obliquity factor (unitless) for satellite i; σ_{vig} is the standard deviation of a normal distribution associated with residual ionospheric uncertainty due to nominal spatial decorrelation ("vig" stands for vertical ionospheric gradient); $x_{aircraft}$ is the horizontal separation between the GBAS ground facility and airplane in kilometers; τ is the time constant of the single-frequency carrier smoothing filter in the GBAS avionics (100 s, same as that used in the ground facility); and $v_{aircraft}$ is the horizontal approach velocity of the airplane in the direction of the GBAS-equipped airport (70 m/s is assumed in this paper).

In this paper, $\sigma_{vig} = 6.4$ mm/km is used as a nominal σ_{vig} value as in [23,24]. (This value represents a root-sum-square combination of the 4.0 mm/km ionospheric value suggested in [15] with a 5.0 mm/km bound on the worst possible tropospheric decorrelation [26].) Starting from this nominal σ_{vig} value, we increase σ_{vig} by 0.1 mm/km, which is the resolution of the broadcast σ_{vig} value specified in the RTCA interface control document (ICD) for GBAS [27], until all unsafe geometries are screened out. This inflation process repeats for x_{DH} of 0–7 km (every 1 km) from the ground facility and aircraft distances from the x_{DH} location (along the same horizontal vector as the ground facility to x_{DH}) of 0–7 km (every 1 km). In this way, the inflated σ_{vig} value screens out all unsafe geometries for the x_{DH} location of every approach direction and any aircraft distance from the x_{DH} location. (Note that the variable x_{DH}, also used in Fig. 4, represents the horizontal distance between an airplane and the ground facility when the airplane reaches the minimum 200 ft decision height for a category I precision approach. The x_{DH} location is specified for each category I approach direction of each airport. The x_{DH} location of every approach direction is considered in our algorithm so that the same software can be used at every airport in CONUS without further modification.) TEL and VAL depend on aircraft distance from the x_{DH} (i.e., $x_{aircraft} - x_{DH}$), as shown in Fig. 4.

Figure 5 shows the result of σ_{vig} inflation at Newark at the same epoch as Fig. 3. The MIEVs and VPLs of the unapproved subset geometries in Fig. 3 (i.e., geometries 7, 10, 12, 17, 19, 23, and 26) are not plotted again, as they were unusable before any inflation. As expected, the inflated VPLs of unsafe geometries with MIEVs exceeding TEL (i.e., geometries 6, 16, and 25) are now above the VAL in Fig. 5. Therefore, all unsafe geometries are properly screened out by σ_{vig} inflation.

Although σ_{vig} inflation meets GBAS integrity requirements, it increases the VPLs of all geometries (including safe ones) and thereby reduces system availability. In Fig. 5, the inflated VPLs screen out some safe geometries as well (i.e., geometries 4, 8, 14, 15, 18, 21, 24, 28, and 29). More importantly, the VPL of the all-in-view satellite geometry (i.e., geometry 1) is also significantly increased. It is expected that an airplane would use the all-in-view satellite

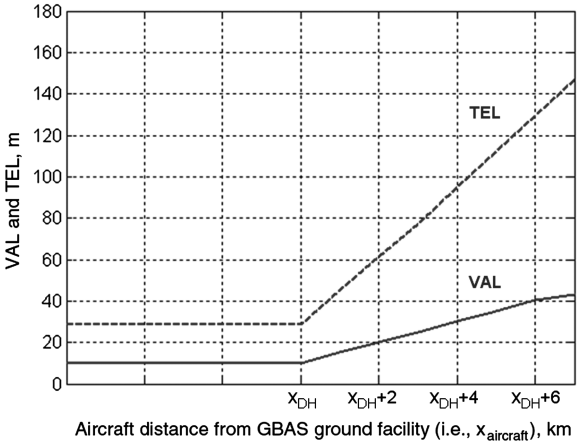

Fig. 4 TEL and VAL for category I GBAS depending on the distance from decision height (x_{DH}). x_{DH} represents the horizontal distance between the ground facility and airplane when the airplane reaches the 200 ft minimum decision height for category I precision approach. (Reproduction of Fig. 7 of [17].)

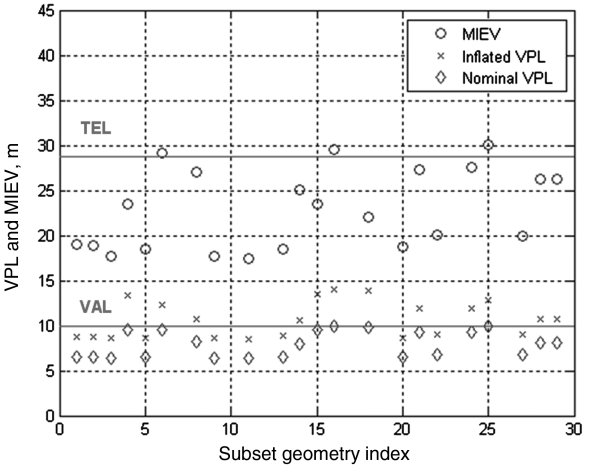

Fig. 5 Geometry screening by σ_{vig} inflation at Newark at the same epoch of Fig. 3. Unsafe geometries with MIEVs exceeding TEL are screened out by inflating their VPLs over VAL. However, σ_{vig} inflation substantially increases the VPLs of all subset geometries, including the all-in-view geometry (geometry 1) and other safe geometries.

geometry more than 95% of the time during its approach. Thus, increasing the VPL of the all-in-view geometry has much more impact on system availability than increasing VPL of other subset geometries.

In general, it is desirable to minimize the VPL inflation of the all-in-view geometry and other safe geometries so that VPL remains below VAL after geometry screening. However, σ_{vig} inflation is not ideal in this purpose, as σ_{vig} is not a satellite-specific parameter. An ideal inflation algorithm would increase the VPLs of all hazardous geometries over VAL, as required for safety, but it should minimize VPL inflation for safe geometries, especially the all-in-view geometry. To do this, we propose a new targeted parameter inflation algorithm in the next section. This method inflates the satellite-specific broadcast parameters $\sigma_{pr_{gnd},i}$ and P_k in Eqs. (5) and (6), respectively, using novel optimization schemes.

III. Targeted Inflation of Broadcast Parameters

A. Satellite-Specific Broadcast Parameters and Optimization Strategy

The basic idea of our targeted inflation algorithm is to exclude unsafe subset geometries by inflating the satellite-specific parameters, $\sigma_{pr_{gnd}}$ and P values, in a way that minimizes the increase in VPL of the all-in-view satellite geometry (recall that, in practice, all-in-view means all satellites approved for use by the ground facility, but this normally includes all satellites in view of the ground facility). This algorithm does not attempt to minimize VPL inflation over all safe subset geometries because the all-in-view geometry has the dominant impact on system availability. The resulting optimization problem is formulated in Eq. (9).

$$\begin{aligned} &\text{Minimize } \max\{\text{VPL}_{H0}, VPL\} \quad \text{for the all-in-view geometry} \\ &\text{Subject to } \max\{VPL_{H0}, \text{VPL}_{\text{eph}}\} \geq \text{VAL} \\ &\quad \text{for each unsafe subset geometry} \end{aligned} \tag{9}$$

Using Eqs. (4) and (5), this optimization problem is expressed in more detail in Eq. (10). The variable N in Eq. (10) is the number of satellites in view of the GBAS ground facility, and N_U is the number of satellites in a given unsafe subset geometry. $S_{U,\text{vert},j}$ represents the vertical position component of the weighted-least-squares projection matrix S for satellite j in a given unsafe subset geometry. We use this notation to emphasize the difference between the S matrix of the all-in-view geometry and the S matrix of an unsafe geometry. These S matrices are usually different even in the number of columns, which are N for all-in-view geometry and N_U for an unsafe geometry. (If the all-in-view geometry is itself unsafe, availability cannot be retained;

thus, optimization of the inflation factors is not relevant.) The other parameters in Eq. (10) are already explained in Eqs. (4) and (5).

$$\text{Minimize } \max\left\{K_{\text{ffmd}}\sqrt{\sum_{i=1}^{N} S_{\text{vert},i}^2\sigma_i^2}, \max_k\left(|S_{\text{vert},k}|x_{\text{aircraft}}P_k + K_{\text{md}_{\text{eph}}}\sqrt{\sum_{i=1}^{N} S_{\text{vert},i}^2\sigma_i^2}\right)\right\} \quad \text{for the all-in-view geometry}$$

$$\text{Subject to } \max\left\{K_{\text{ffmd}}\sqrt{\sum_{j=1}^{N_U} S_{U,\text{vert},j}^2\sigma_j^2}, \max_k\left(|S_{U,\text{vert},k}|x_{\text{aircraft}}P_k + K_{\text{md}_{\text{eph}}}\sqrt{\sum_{j=1}^{N_U} S_{U,\text{vert},j}^2\sigma_j^2}\right)\right\} \geq \text{VAL} \quad \text{for each unsafe subset geometry} \tag{10}$$

Considering the expressions of S matrix and σ_i^2 in Eqs. (3) and (6), respectively, this optimization problem is highly nonlinear in terms of the optimization parameters $\sigma_{pr_{\text{gnd}},i}$ and P_k. To be useful, geometry screening must be performed in real time by the GBAS ground facility, and it would be difficult to solve and verify the safety of solutions for this nonlinear optimization problem for real-time operations. Thus, we suggest a practical suboptimal algorithm that protects system integrity and provides significant availability benefit over σ_{vig} inflation.

To simplify the complex optimization problem presented above, we separate the problem into two independent optimization problems: one for VPL_{H0} and the other for VPL_{eph}. Figure 6 shows the typical trends of VPL_{H0} and VPL_{eph} as a function of increasing separation. For a small separation between the ground facility and airplane (i.e., for small x_{aircraft}), VPL_{H0} dominates, but VPL_{eph} dominates for large x_{aircraft}. Hence, Eq. (9) can be separated into the two optimization problems defined by Eqs. (11) and (12). However, the distance to the point where the VPL_{H0} and VPL_{eph} lines cross (define this as x_{cross}) is dependent on the optimization parameters $\sigma_{pr_{\text{gnd}},i}$ and P_k in general. Thus, Eqs. (11) and (12) cannot be solved independently. To formulate two independent optimization problems, we assign a fixed x_{cross} from 1 to 14 km (every 1 km) to cover the whole range of x_{aircraft} for category I approaches. These two independent optimization problems isolate $\sigma_{pr_{\text{gnd}}}$ optimization to one problem and P value optimization to the other problem. After obtaining a solution for each value of x_{cross}, a final optimization solution is selected among the set of valid solutions optimized for each value of x_{cross}. Detailed explanations to solve Eqs. (11) and (12) and to obtain a final optimization solution are given in the following subsections.

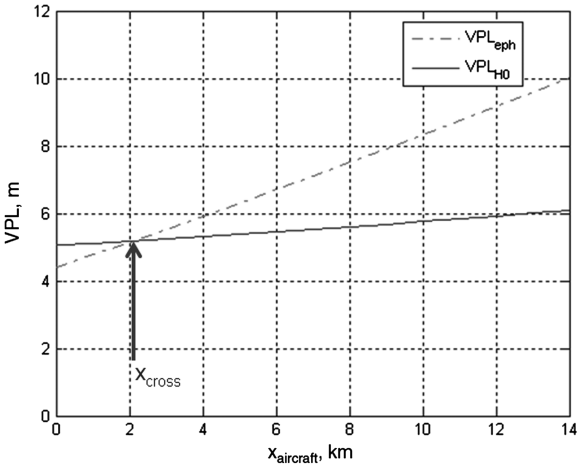

Fig. 6 Typical trend of VPH_{H0} and VPL_{eph} depending on the distance between the GBAS ground facility and airplane. VPH_{H0} dominates for small x_{aircraft} and VPL_{eph} dominates for large x_{aircraft}. The crossing distance x_{cross} of two VPL curves has a nonlinear relationship with many parameters, including our optimization parameters (i.e., $\sigma_{pr_{\text{gnd}}}$ and P values).

$$\text{Minimize } \text{VPL}_{H0} \quad \text{for all-in-view geometry,} \quad \text{if } x_{\text{aircraft}} \leq x_{\text{cross}}$$
$$\text{Subject to } \text{VPL}_{H0} \geq \text{VAL} \quad \text{for each unsafe subset geometry} \tag{11}$$

$$\text{Minimize } \text{VPL}_{\text{eph}} \quad \text{for all-in-view geometry,} \quad \text{if } x_{\text{aircraft}} > x_{\text{cross}}$$
$$\text{Subject to } \text{VPL}_{\text{eph}} \geq \text{VAL} \quad \text{for each unsafe subset geometry} \tag{12}$$

B. $\sigma_{pr_{\text{gnd}}}$ Inflation by VPL_{H0} Optimization

This subsection suggests a way to simplify and solve the optimization problem in Eq. (11), which is the case where $x_{\text{aircraft}} \leq x_{\text{cross}}$ for a given x_{cross}. Equation (11) can be expressed in detail as Eq. (13). By this VPL_{H0} optimization, an optimized σ_i^2 for satellite i can be obtained. Then, the optimization parameter $\sigma_{pr_{\text{gnd}},i}$ can be calculated subsequently using Eq. (6).

$$\text{Minimize } K_{\text{ffmd}}\sqrt{\sum_{i=1}^{N} S_{\text{vert},i}^2\sigma_i^2} \quad \text{for all-in-view geometry}$$
$$\text{Subject to } K_{\text{ffmd}}\sqrt{\sum_{j=1}^{N_U} S_{U,\text{vert},j}^2\sigma_j^2} \geq \text{VAL} \quad \text{for each unsafe subset geometry} \tag{13}$$

Equation (13) is still a nonlinear optimization problem because σ_i^2 affects the weighting matrix used to compute S in Eq. (3). To linearize this equation, $\sigma_{pr_{\text{gnd}},i}$ is fixed at the nominal broadcast value (without any inflation) when the S matrices are first calculated. Fixing S matrices based on the nominal $\sigma_{pr_{\text{gnd}},i}$ is an acceptable approximation because the S matrix values have only a second-order effect on position solutions and protection levels.

Then, Eq. (13) can be expressed as Eq. (14), which is an LP optimization problem [28] in terms of σ_i^2 because the S matrices are now constant. $\sigma_{pr_{\text{gnd}},i,0}$ in Eq. (14) represents the nominal $\sigma_{pr_{\text{gnd}},i}$ before inflation, which is preestablished at each GBAS site and typically varies with satellite elevation. The ICD for GBAS [27] specifies the maximum broadcast value of $\sigma_{pr_{\text{gnd}}}$, which is 5.08 m. Thus, it provides another constraint equation for each satellite, as shown in Eq. (14). The lower-bound constraint is from the nominal value before inflation (i.e., $\sigma_{pr_{\text{gnd}},i,0}$) and the upper-bound constraint is from the maximum broadcast value (i.e., 5.08 m). In this algorithm, $\sigma_{\text{tropo},i}$, $\sigma_{pr_{\text{air}},i}$, and $\sigma_{\text{iono},i}$ are nominal broadcast values that are not subject to inflation. Figure 7 shows the elevation-dependent curves of nominal $\sigma_{pr_{\text{gnd}}}$ and $\sigma_{pr_{\text{air}}}$ used in this paper (see [17] for details).

$$\text{Minimize } \sum_{i=1}^{N} S_{\text{vert},i}^2\sigma_i^2 \quad \text{for the all-in-view geometry}$$
$$\text{Subject to } -\sum_{j=1}^{N_U} S_{U,\text{vert},j}^2\sigma_j^2 \leq -\left(\frac{\text{VAL}}{K_{\text{ffmd}}}\right)^2$$
$$\text{for each unsafe subset geometry}$$
$$\sigma_{pr_{\text{gnd}},i,0}^2 + \sigma_{\text{tropo},i}^2 + \sigma_{pr_{\text{air}},i}^2 + \sigma_{\text{iono},i}^2 \leq \sigma_i^2 \leq 5.08^2 + \sigma_{\text{tropo},i}^2 + \sigma_{pr_{\text{air}},i}^2 + \sigma_{\text{iono},i}^2 \quad \text{for satellite } i \tag{14}$$

Because Eq. (14) is an LP in terms of σ_i^2, it can be solved very quickly. Once an optimized σ_i^2 for satellite i is obtained by solving this LP, an optimally inflated $\sigma_{pr_{\text{gnd}},i}$ for satellite i is obtained from Eq. (6). Note that the optimal solution of this linearized problem in Eq. (14) is suboptimal to the original nonlinear optimization problem in Eq. (13). Because we fixed the S matrices as constants for linearization, the suboptimal solution may not satisfy the constraint of the original problem in Eq. (13). This is unacceptable because of

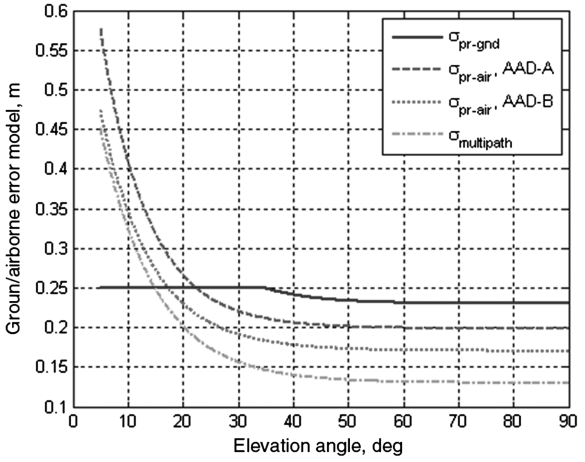

Fig. 7 Elevation-dependant nominal error models used in this paper. (Reproduction of Fig. 8 of [17].)

the possibility that unsafe geometries may not be removed if the inflated $\sigma_{pr_{\text{gnd}},i}$ does not satisfy the original constraints. Thus, a validation and adjustment process is needed and will be discussed in Sec. III.D, after explaining VPL_{eph} optimization in the following subsection.

C. *P* Value Inflation by VPL_{eph} Optimization

The previous subsection discussed the case of $x_{\text{aircraft}} \leq x_{\text{cross}}$. The other case, in which $x_{\text{aircraft}} > x_{\text{cross}}$ [Eq. (12)], is considered in this subsection. This VPL_{eph} optimization problem is expressed in detail in Eq. (15), which is also a nonlinear optimization problem.

$$\text{Minimize } \max_k(|S_{\text{vert},k}|P_k) \times x_{\text{aircraft}} + K_{\text{md}_{\text{eph}}}\sqrt{\sum_{i=1}^{N} S_{\text{vert},i}^2\sigma_i^2}$$

for the all-in-view geometry

$$\text{Subject to } \max_k(|S_{U,\text{vert},k}|P_k) \times x_{\text{aircraft}} + K_{\text{md}_{\text{eph}}}\sqrt{\sum_{j=1}^{N_U} S_{U,\text{vert},j}^2\sigma_j^2} \geq \text{VAL}$$

for each unsafe subset geometry (15)

We set $\sigma_{pr_{\text{gnd}},i}$ to be the nominal broadcast value without any inflation. Then, as before, the S matrices and σ_i values are now constant for each geometry. Note that, instead of the nominal broadcast value, the optimal $\sigma_{pr_{\text{gnd}},i}$ values obtained from Eq. (14) could be used to set the S matrices and σ_i. In this approach, Eq. (14) must be solved before Eq. (15). However, this approach does not demonstrate improved performance in practice. Hence, the nominal broadcast value of $\sigma_{pr_{\text{gnd}},i}$ is used to initialize the algorithm, and Eqs. (14) and (15) can be solved in either order or in parallel if parallel processors are available.

Furthermore, the nominal critical satellite, which is defined as the satellite k that results in the maximum value of $|S_{\text{vert},k}|P_k$ before parameter inflation, is used as critical satellite even after inflation is implemented. Thus, the maximize operation in Eq. (15) can be removed because the critical satellite is now fixed a priori. This simplification is not always correct but works well in practice. Although a different satellite could become the true critical satellite (the one that maximizes $|S_{\text{vert},k}|P_k$) after P value is inflated, other satellites require more P-value inflation to increase VPL_{eph} than the nominal critical satellite. For this reason, inflation of the nominal critical satellite's P value is the simplest way to inflate VPL_{eph}.

With these approximations, Eq. (15) can be reduced to an LP in terms of P values, as in Eq. (16). The satellite index C in Eq. (16) represents the a priori critical satellite of the all-in-view geometry, and the satellite index χ represents the a priori critical satellite of each unsafe subset geometry. The maximum broadcast P value (i.e., 0.001275 m/m) is specified by the ICD [27], which provides another constraint equation for each satellite. P_0 in Eq. (16) represents the preinflation P value; $P_0 = 0.00014$ is used for the targeted inflation in this paper. By solving this LP, an optimally inflated P value for each satellite is obtained.

$$\text{Minimize} |S_{\text{vert},C}|P_C \quad \text{for all-in-view geometry}$$

$$\text{Subject to } -|S_{U,\text{vert},\chi}|P_\chi \leq \frac{K_{\text{md}_{\text{eph}}}\sqrt{\sum_{j=1}^{N_U} S_{U,vert,j}^2} - \text{VAL}}{x_{\text{aircraft}}}$$

for each unsafe subset geometry

$$P_0 \leq P_i \leq 0.001275 \quad \text{for satellite } i \tag{16}$$

The preinflation P value of 0.00014 is based on the maximum P value needed to protect against ephemeris faults. This P value is calculated by dividing the minimum detectable error of the ephemeris monitors of about 2700 m (in 3-D satellite orbit space) by the minimum range from GBAS ground facility to GPS satellite (about 2.018×10^7 m; note that using the minimum range maximizes the resulting P value) and rounding up [29,30].

For a given value of x_{cross}, a set of optimally inflated values of $\sigma_{pr_{\text{gnd}},i}$ and P_i is obtained from Eqs. (14) and (16). We consider x_{DH} from 0 to 7 km (every 1 km) and x_{aircraft} from x_{DH} to $x_{\text{DH}} + 7$ km (every 1 km), which was also considered in the σ_{vig} inflation in Sec. II.B, to cover the whole range of possible aircraft locations. Among these 64 different values of $\sigma_{pr_{\text{gnd}},i}$ and P_i for satellite i from eight x_{DH} distances and eight x_{aircraft} distances, the maximum value is taken for each satellite to be conservative. Then, the obtained $\sigma_{pr_{\text{gnd}},i}$ and P_i values will screen out all unsafe geometries within the whole distance range.

Recall that, because each solution generated in this manner is (approximately) optimal for a single value of x_{cross}, this process is repeated over the set of possible values of x_{cross} from 1 to 14 km (again at 1 km intervals). Any of the resulting 14 sets of obtained parameters from 14 x_{cross} distances protects integrity for the whole range of x_{DH} and x_{aircraft} distances, but the suitability of each set depends on the match between the assumed and true (unknown) value of x_{cross}. Therefore, the best (optimal) set of parameters is selected by computing the VPL of the all-in-view geometry at the x_{DH} and x_{aircraft} using each set of $\sigma_{pr_{\text{gnd}},i}$ and P_i obtained for each of the 14 assumed values of x_{cross}.

The set that gives the minimum VPL at the x_{DH} and x_{aircraft} distances is selected as the best set of $\sigma_{pr_{\text{gnd}},i}$ and P_i. Although the x_{DH} and x_{aircraft} distances for this selection process can be any values of interest, $x_{\text{DH}} = 6$ km and $x_{\text{aircraft}} = 6$ km is usually the limiting case requiring the largest parameter inflations in practice. Thus, the best set of $\sigma_{pr_{\text{gnd}},i}$ and P_i is selected based on $x_{\text{DH}} = 6$ km and $x_{\text{aircraft}} = 6$ km in this paper to provide the most availability benefit from this algorithm. $x_{\text{DH}} = 6$ km is expected to be the limiting siting case, which means that x_{DH} as large as 6 km (with $x_{\text{aircraft}} = x_{\text{DH}}$) may be allowed but not any larger (with a few exceptions). Therefore, $x_{\text{DH}} = 6$ km is the limiting case for general studies as in this paper. However, the best selection for a given airport is the largest x_{DH} separation supported at that airport (and $x_{\text{aircraft}} = x_{\text{DH}}$). For most airports, that will be between 3 and 5 km.

D. Validation and Adjustment of Broadcast Parameters

Although the obtained set of $\sigma_{pr_{\text{gnd}},i}$ and P_i from Secs. III.B and III.C is expected to remove all unsafe subset geometries over the whole range of x_{DH} and x_{aircraft}, it is not necessarily true because of the approximations for linearization mentioned in Secs. III.B and III.C. Thus, the obtained parameters need to be validated and adjusted if the obtained parameters do not remove all unsafe subset geometries over the whole range. To validate the obtained parameters, the original constraint equations in Eqs. (13) and (15), repeated below as Eqs. (17) and (18), are checked with the inflated $\sigma_{pr_{\text{gnd}},i}$ and P_i values over the whole range of x_{DH} and x_{aircraft}.

$$K_{\text{ffmd}}\sqrt{\sum_{j=1}^{N_U} S_{U,\text{vert},j}^2\sigma_j^2} \geq \text{VAL} \quad \text{for each unsafe subset geometry} \tag{17}$$

$$\max_k(|S_{U,\text{vert},k}|P_k) \times x_{\text{aircraft}} + K_{\text{md}_{\text{eph}}}\sqrt{\sum_{j=1}^{N_U} S_{U,\text{vert},j}^2\sigma_j^2} \geq \text{VAL}$$

for each unsafe subset geometry (18)

Note that an unsafe subset geometry will be screened out if either Eq. (17) or Eq. (18) is satisfied. They do not need to be simultaneously satisfied. If neither constraint is satisfied for an unsafe subset geometry, adjustment of $\sigma_{pr_{\text{gnd}},i}$ or P_i is required.

If the left-hand side of Eq. (17) is larger than the left-hand side of Eq. (18) (in other words, if Eq. (17) dominates for an unsafe subset geometry at a certain x_{DH} and x_{aircraft}), we increase the obtained $\sigma_{pr_{\text{gnd}}}$ values of all satellites within the subset geometry by 0.02 m, which is the resolution (and thus the minimum possible increment) of the broadcast $\sigma_{pr_{\text{gnd}}}$ specified in [27], and Eq. (17) is checked again until it is satisfied. The S matrix must be recalculated (with adjusted $\sigma_{pr_{\text{gnd}}}$ values) each time. This incremental parameter adjustment is preferred to iteratively solving LP with an updated S matrix because of its computational efficiency. Similarly, if Eq. (18) dominates for an unsafe subset geometry, we increase the P value of the critical satellite by 0.000005 m/m, which is the resolution (and minimum increment) of each broadcast P value [27], until Eq. (18) is satisfied. Note that the critical satellite is the satellite that provides the maximum value of $|S_{U,\text{vert},k}|P_k$ among all satellites in the given subset geometry based upon the inflated P values before adjustment occurs.

In practice, 60% of the 1440 epochs in a 24 hr period (1 min interval) at Newark Liberty International Airport require parameter inflation. Among the 60% of total epochs, 22% require additional parameter adjustments after the targeted inflation. For those epochs needing parameter adjustments, the average number of geometries requiring $\sigma_{pr_{\text{gnd}}}$ adjustments is 0.2 per epoch, and the average number of geometries requiring P-value adjustments is 1.0 per epoch. In other words, although 13.2% of each day's epochs (60% × 22%= 13.2%) require parameter adjustments, an average of one subset geometry per epoch requires P-value adjustments, and $\sigma_{pr_{\text{gnd}}}$ adjustments are needed roughly once every five epochs. This implies that the approximations used to formulate the LPs in Eqs. (14) and (16) are close enough to correct to generate near-optimal results.

For the epochs requiring adjustment, the average number of increments of $\sigma_{pr_{\text{gnd}}}$ is 0.3 per epoch, and the average number of increments of P values is 9.4 per epoch. In other words, although an average of only one geometry per epoch requires P-value adjustments, an average of between nine and ten P-value increments are needed. This means that the minimum P-value increment based on the resolution in the ICD [27] (i.e., 0.000005 m/m) could be increased in practice. If the increment were changed to 0.000025 m/m, for example, about two P-value increments per epoch would be sufficient. However, this change may not noticeably reduce total computational time because the validation and adjustment process is not computationally expensive. A flowchart that summarizes the implementation of the targeted inflation algorithm is given in Fig. 8.

E. Effectiveness of the Targeted Inflation Algorithm

Through this parameter validation and adjustment, the final broadcast $\sigma_{pr_{\text{gnd}}}$ and P values of each satellite are determined, and these have been validated to screen out all unsafe geometries as required. For comparison, the inflated broadcast parameters generated by our targeted inflation algorithm at Newark at the same epoch as Figs. 3 and 5 are shown in Table 1 along with their nominal values before inflation. For this epoch, significant $\sigma_{pr_{\text{gnd}}}$ inflation is needed for satellites 1, 2, and 4, but P-value inflation is not necessary because the constraint in Eq. (15) is satisfied without any P-value inflation when $x_{\text{cross}} = 9$ km.

Table 2 shows another set of inflated parameters when $x_{\text{cross}} = 1$ km for comparison. The case of $x_{\text{cross}} = 1$ km means that $\sigma_{pr_{\text{gnd}}}$ inflation (i.e., VPL_{H0} inflation) screens out unsafe geometries for $x_{\text{cross}} \leq 1$ km, and P-value inflation (i.e., VPL_{eph} inflation) screens out unsafe geometries for $x_{\text{cross}} > 1$ km. Because P-value inflation has the most responsibility in this case, $\sigma_{pr_{\text{gnd}},i}$ values are not highly

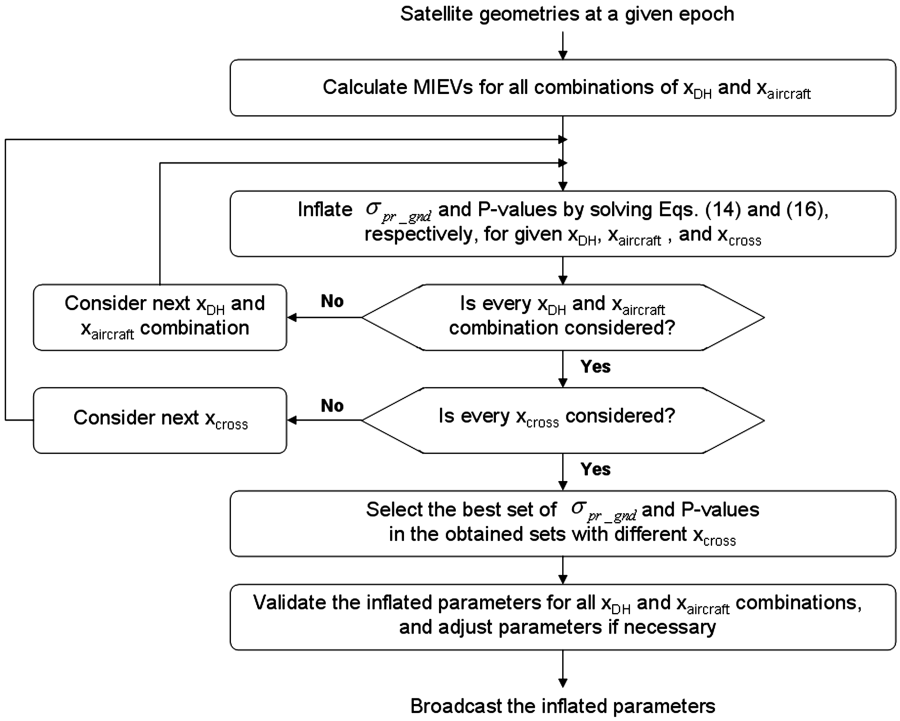

Fig. 8 Flowchart of the targeted inflation algorithm.

Table 1 Inflated parameters by targeted inflation at the same epoch of Figs. 3 and 5 (this best set of parameters is obtained with $x_{\text{cross}} = 9$ km)

Satellite index		1	2	3	4	5	6	7
$\sigma_{pr_{\text{gnd},i}}$, mm/km	Nominal	0.26	0.26	0.24	0.24	0.26	0.24	0.24
	Inflated	0.84	0.72	0.26	1.08	0.28	0.26	0.26
P_i, m/m)	Nominal	0.000140	0.000140	0.000140	0.000140	0.000140	0.000140	0.000140
	Inflated	0.000140	0.000140	0.000140	0.000140	0.000140	0.000140	0.000140

Table 2 Inflated parameters by targeted inflation at the same epoch of Table 1 with $x_{\text{cross}} = 1$ km for comparison

Satellite index		1	2	3	4	5	6	7
$\sigma_{pr_{\text{gnd},i}}$, mm/km)	Nominal	0.26	0.26	0.24	0.24	0.26	0.24	0.24
	Inflated	0.28	0.28	0.26	0.58	0.28	0.26	0.26
P_i, m/m)	Nominal	0.000140	0.000140	0.000140	0.000140	0.000140	0.000140	0.000140
	Inflated	0.000705	0.000825	0.000400	0.000705	0.000395	0.000765	0.000330

inflated but P_i values are significantly inflated, as shown in Table 2. This set of inflated parameters in Table 2 is not selected as the best set because it provides a VPL of 9.17 m at $x_{\text{DH}} = 6$ km and $x_{\text{aircraft}} = 6$ km for the all-in-view geometry. On the other hand, the best set of parameters in Table 1 (for $x_{\text{cross}} = 9$ km) gives an all-in-view VPL of 6.34 m and thus gives better availability.

With these inflated parameters in Table 1, the VPLs of all subset geometries at this epoch are plotted in Fig. 9. The inflated VPLs properly screen out all unsafe geometries with MIEVs exceeding TEL (i.e., geometries 6, 16, and 25) as expected. Compared to Fig. 5, Fig. 9 shows significant improvement. The VPL of the all-in-view geometry (i.e., geometry 1) is not noticeably increased in Fig. 9, even after parameter inflation. As shown in Table 3, the VPL of the all-in-view geometry is increased slightly from 6.27 to 6.34 m by targeted inflation (Fig. 9), but σ_{vig} inflation (Fig. 5) increases the VPL of the all-in-view geometry dramatically from 6.27 to 8.82 m. In the σ_{vig} inflation algorithm, the single inflation parameter affecting all satellites (i.e., σ_{vig}) is inflated from 6.4 mm/km to 14.1 mm/km to screen out all unsafe geometries. However, in the targeted inflation algorithm, satellite-specific parameters (i.e., $\sigma_{pr_{\text{gnd}}}$ and P value) are inflated in a way to minimize the required increase in the all-in-view VPL.

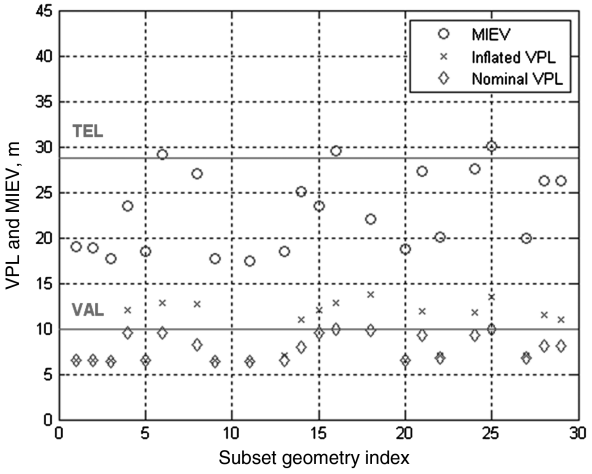

Fig. 9 Geometry screening by targeted inflation at Newark at the same epoch as Figs. 3 and 5. Even though VPLs of unsafe geometries with MIEVs exceeding TEL are inflated over VAL as required, the VPL of the all-in-view geometry (i.e., geometry 1) is not noticeably inflated. This preserves availability and is a significant benefit over σ_{vig} inflation in Fig. 5.

Table 4 shows why this approach to targeted inflation results in a much lower VPL than σ_{vig} inflation at this epoch, although targeted inflation significantly increases $\sigma_{pr_{\text{gnd},i}}$ for satellites 1, 2, and 4. After σ_{vig} inflation, σ_i for all satellites uniformly increases by 30 to 55%. On the other hand, σ_i of the four satellites other than satellites 1, 2, and 4 only changes slightly (less than 5%) after targeted inflation. The variations of $|S_{\text{vert},i}|$ do not show a clear trend after σ_{vig} inflation. However, the $|S_{\text{vert},i}|$ values of satellites 1, 2, and 4 are noticeably decreased after targeted inflation (Table 4). These are the satellites whose σ_i values are significantly increased by targeted inflation. This paper does not attempt to explain this trend mathematically, but it is intuitively understandable. The S matrix in Eq. (3) is the weighted-least-squares projection matrix. The purpose of weighted-least-squares is to give greater weight to better measurements with less noise (i.e., smaller σ_i). Thus, if the σ_i values of a few satellites are significantly higher than others, the components of the S matrix for those satellites should be decreased. (However, if the σ_i values for all satellites are uniformly increased, the weighted-least-squares method does not show this trend.) As a result, this weighting scheme reduces the inflation of $S^2_{\text{vert},i}\sigma_i^2$ used for VPL calculations in Eqs. (4) and (5) even though targeted inflation significantly increases σ_i for a few satellites. This is the main reason why the VPL of the all-in-view geometry is slightly increased from 6.27 to 6.34 m by targeted inflation at this epoch, whereas σ_{vig} inflation significantly increases this VPL from 6.27 to 8.82 m (Table 3).

Because the all-in-view geometry has the dominant impact on overall user availability, the minimal inflation of the all-in-view VPL from targeted inflation provides a significant availability benefit. Although there are more optimization parameters for targeted inflation than for σ_{vig} inflation (i.e., $2N$ parameters vs one parameter, $N = 7$ in the given example), and the algorithm is more complex, the resulting availability improvement has great operational, economic, and safety benefits.

IV. Performance of the Targeted Inflation Algorithm

We have used a single epoch at Newark Liberty International Airport as an example to explain and compare the σ_{vig} inflation and targeted inflation algorithms in previous sections. In this section, availability analyses for a 24 hr period at Newark Liberty International Airport and Memphis International Airport are presented. Practical issues for implementing targeted inflation in real-time operations are also discussed.

A. Availability Improvement from Targeted Inflation

For the purposes of comparison, the availability analyses of this section use the same simulation setting as in [17] and as previously used in this paper. Specifically, the standard RTCA 24-satellite GPS

Table 3 Comparison of inflated VPLs of the all-in-view geometry for σ_{vig} inflation and targeted inflation at the same epoch of Figs. 5 and 8

	σ_{vig} inflation			Targeted $\sigma_{pr_{gnd}}$ and P-value inflation		
	VPL_{H0}	VPL_{eph}	VPL	VPL_{H0}	VPL_{eph}	VPL
Nominal value, m	5.45	6.27	6.27	5.45	6.27	6.27
Inflated value, m	7.71	8.82	8.82	5.67	6.34	6.34

Table 4 Comparison of σ_i, $|S_{vert,i}|$, and $S^2_{vert,i}\sigma^2_i$ of the all-in-view geometry at the same epoch of Table 3 (the percentage changes are with respect to nominal values)

	Satellite index	1	2	3	4	5	6	7
σ_i, m	Nominal	0.3708	0.3787	0.3252	0.3325	0.6314	0.3353	0.3461
	After σ_{vig}	0.5311	0.5531	0.4231	0.4481	0.9795	0.4570	0.4903
	inflation	(+43%)	(+46%)	(+30%)	(+35%)	(+55%)	(+36%)	(+42%)
	After targeted inflation	0.8806	0.7709	0.3403	1.1043	0.6399	0.3499	0.3602
		(+137%)[a]	(+104%)[a]	(+5%)	(+232%)[a]	(+1%)	(+4%)	(+4%)
$\lvert S_{vert,i}\rvert$	Nominal	0.1007	0.2395	1.8193	0.0756	0.8997	0.4594	1.1647
	After σ_{vig}	0.0517	0.4031	1.9563	0.1317	0.8102	0.4921	1.1550
	inflation	(−49%)	(+68%)	(+8%)	(+74%)	(−10%)	(+7%)	(−1%)
	After targeted inflation	0.0554	0.0871	1.6720	0.0205	0.9547	0.5668	1.2319
		(−45%)[a]	(−64%)[a]	(−8%)	(−73%)[a]	(+6%)	(+23%)	(+6%)
$S^2_{vert,i}\sigma^2_i$, m^2	Nominal	0.0014	0.0082	0.3501	0.0006	0.3227	0.0237	0.1625
	After σ_{vig}	0.0008	0.0497	0.6851	0.0035	0.6298	0.0506	0.3206
	inflation	(−43%)	(+506%)	(+96%)	(+483%)	(+95%)	(+113%)	(+97%)
	After targeted inflation	0.0024	0.0045	0.3237	0.0005	0.3733	0.0393	0.1969
		(+71%)	(−45%)	(−8%)	(−17%)	(+16%)	(+66%)	(+21%)

[a]Although σ_i of these satellites are significantly increased after targeted inflation, their $|S_{vert,i}|$ are noticeably decreased.

constellation (Table B-1 in [31]) is assumed with all 24 satellites being healthy. Parameter inflation is performed at one-minute intervals over 24 hr (i.e., a total of 1440 epochs). x_{DH} distances from 0 to 7 km (every 1 km) and $x_{aircraft}$ of x_{DH} to $x_{DH} + 7$ km (every 1 km) are considered for parameter inflation. For nominal values before inflation, $\sigma_{vig} = 6.4$ mm/km, $P = 0.00014$, and $\sigma_{pr_{gnd}}$ follow Fig. 7. Also, the CONUS ionospheric threat model [14] is applied. A slightly larger fixed P value ($P = 0.00018$) is used for σ_{vig} inflation to assist the effectiveness of the algorithm as in [17,23,24]. However, this adjustment is not necessary for targeted inflation because optimized P values are calculated by the targeted inflation algorithm itself.

Figure 10 shows VPL for the all-in-view geometry at $x_{DH} = 6$ km and $x_{aircraft} = 6$ km (i.e., the aircraft is at the x_{DH}) at Newark Liberty International Airport. For the MIEV calculation for geometry screening, $c = 1.0$ for Eq. (2) is used for comparison even though it is unnecessarily conservative, as it is widely assumed in the literature (e.g., [23,24]). If anomalous ionospheric events did not exist at all, geometry screening would not be necessary, and the all-in-view geometry would have 100% availability under these assumptions. This result is shown in Fig. 10, where the VPL curve without inflation is always lower than VAL. Given the threat posed by anomalous ionospheric events, if geometry screening by σ_{vig} inflation is applied, the inflated VPLs exceeds VAL at several epochs, and only 97.4% availability would be obtained. On the other hand, if the targeted inflation algorithm proposed in this paper is applied, the inflated VPLs are always lower than VAL, meaning the 100% availability of the uninflated condition is maintained for the all-in-view geometry. Further, the targeted inflation generally provides much larger margin between VAL and the inflated VPLs compared with the σ_{vig} inflation case.

Figure 11 shows another result for Newark using $c = 0.5$ in Eq. (2) for a more realistic MIEV calculation, as suggested in [17]. This choice of c factor provides conservative protection against all observed ionospheric front scenarios in CONUS. In this case, σ_{vig} inflation also provides 100% availability for the all-in-view geometry, as reducing the c factor reduces MIEV, which results in less need for inflation in general. However, targeted inflation provides even more margin between inflated VPLs and VAL compared to σ_{vig} inflation. This additional margin means that 100% availability with integrity is more likely to be maintained under poorer circumstances than those assumed here, such as outages of one or more GPS satellites. The same analyses have been performed at Memphis International Airport as well. The results in Figs. 12 and 13 with $c = 1.0$ and $c = 0.5$, respectively, at Memphis demonstrate similar availability improvements and larger margins relative to VAL from the targeted inflation algorithm.

Although targeted inflation generally provides smaller VPLs, it was observed for a few epochs at Newark and Memphis that σ_{vig} inflation provides slightly smaller VPLs (two epochs out of 1440 epochs at Newark when $c = 1.0$ or $c = 0.5$, eight epochs at Memphis when $c = 1.0$, and three epochs at Memphis when $c = 0.5$). This is because the targeted inflation algorithm does not

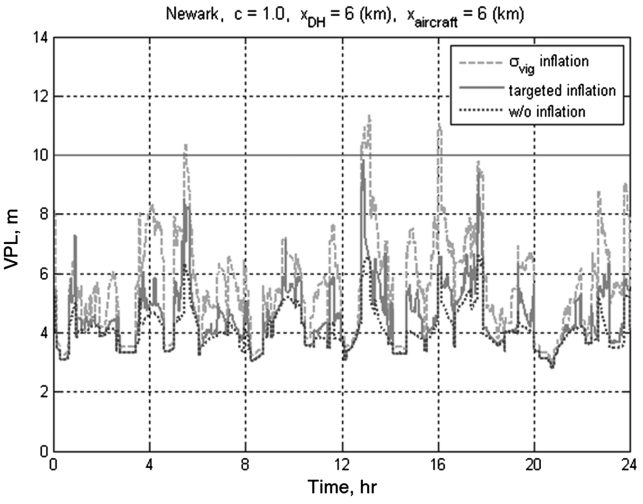

Fig. 10 Availability analysis at Newark Liberty International Airport for the all-in-view satellite geometry. Inflated VPLs from targeted inflation are always lower than VAL. Thus, 100% availability for the all-in-view geometry remains attainable under these assumptions, despite the need for geometry screening. σ_{vig} inflation, however, provides only 97.4% availability.

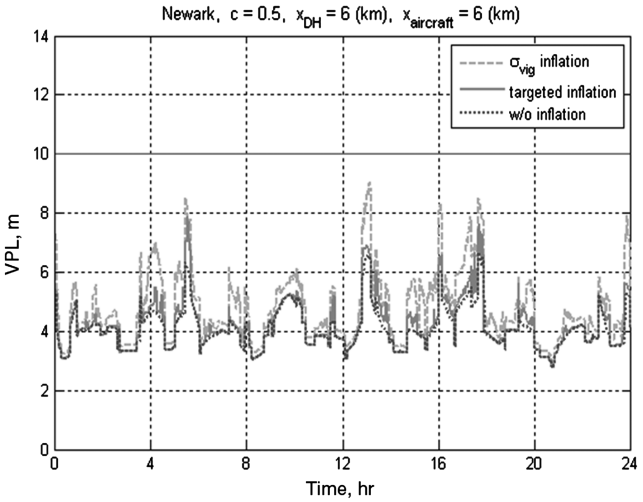

Fig. 11 Availability analysis at Newark with $c = 0.5$ for MIEV calculation. Although σ_{vig} inflation also provides 100% availability for the all-in-view geometry, targeted inflation provides much larger margin between the inflated VPLs and VAL.

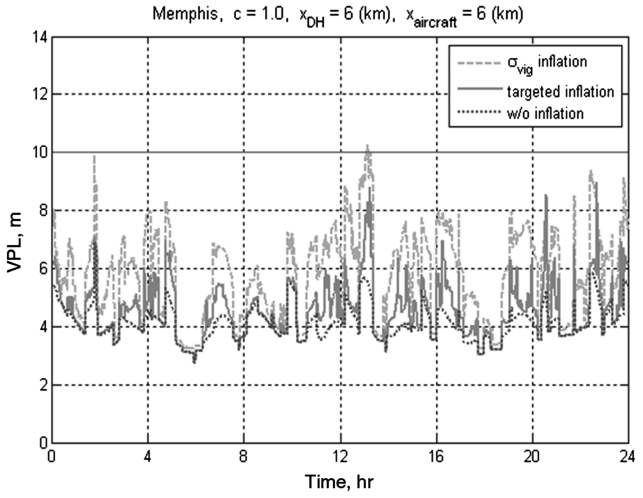

Fig. 12 Availability analysis at Memphis with $c = 1.0$ for MIEV calculation. This result is very similar to the Newark case shown in Fig. 10.

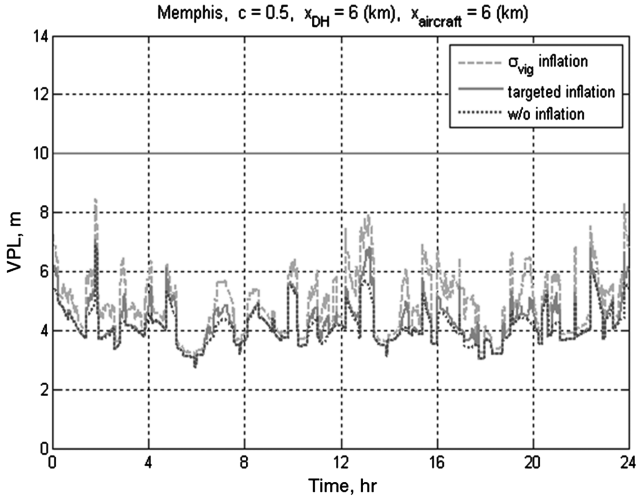

Fig. 13 Availability analysis at Memphis with the $c = 0.5$ for MIEV calculation. This result is very similar to the Newark case shown in Fig. 11.

necessarily provide globally optimal solutions, as explained previously. Deriving a simplified, solvable optimization problem requires both linearization and, more importantly, the reduction of a single joint optimization problem over both $\sigma_{pr_{gnd}}$ and P values into two distinct problems addressing $\sigma_{pr_{gnd}}$ and P values separately. Even if the original nonlinear joint optimization problem over $\sigma_{pr_{gnd}}$ and P values were confronted, the exclusion of σ_{vig} from the optimization problem creates a further limitation. Although the resulting $\sigma_{pr_{gnd}}$ and P values are suboptimal to those that would solve the original nonlinear optimization problems, the availability analyses and results in Figs. 10–13 confirm that this approach provides significant and worthwhile improvements over σ_{vig} inflation in general.

B. Practical Considerations for Real-Time Operations

As described earlier, a suboptimal algorithm is necessary because it must support real-time operations in the GBAS ground facility. In practice, this means that the entire inflation and optimization procedure must be repeated at 60 s intervals. Shorter intervals (10–15 s) are much better, as longer intervals allow more satellite motion (and thus more changes in satellite geometry) to occur during the interval.

As an example, we measured the (offline) computational times of the two algorithms examined in this paper to provide inflation parameters for one epoch of real time using a PC with an Intel Core i7 950 CPU. These inflation algorithms are both implemented with Matlab scripts. For one epoch, σ_{vig} inflation takes 0.7 s, whereas targeted $\sigma_{pr_{gnd}}$ and P-value inflation takes 1.7 s. These computational times include parameter inflation calculations only; they do not include the elements of the geometry-screening process, such as MIEV calculations, that are common to both inflation algorithms. In fact, MIEV calculation for this epoch takes 9.2 s. Thus, parameter inflation is not the most computationally expensive component of geometry screening.

It is not easy to extrapolate these results to a GBAS ground system because of the many differences between the offline Matlab context and a real-time environment. Operational software runs in a specialized real-time operating system and is implemented in coding languages such as C/C++, which are generally more than an order of magnitude faster than Matlab. On the other hand, most of the processing load of a GBAS ground system would be dedicated to the calculations that must be repeated every 2 Hz measurement epoch. A form of σ_{vig} inflation is already implemented by the Honeywell SLS-4000 category I LAAS ground facility using a 1 min update rate, but this is known to stress the processing budget of the SLS-4000 [20]. Therefore, it is likely that careful coding and software planning will be needed to integrate targeted inflation into future GBAS ground stations.

Other practical issues not yet revealed in the simulations performed to date must be handled in advance to maintain confidence that successful geometry screening can be carried out under all conditions. For example, it is theoretically possible that the LPs defined in Eqs. (14) and (16) will not have valid solutions, although no such cases have been observed in our analyses at Newark Liberty International Airport and Memphis International Airport. If this were to happen at a particular location and time interval, the inflation algorithm can temporarily switch to σ_{vig} inflation. This use of σ_{vig} inflation in a backup role adds slightly to the overall computational burden, but this can be minimized by computing inflated σ_{vig} values at slower update rates (because they are unlikely to be needed).

Another potential use of σ_{vig} inflation in a backup role arises from the validation and adjustment procedure described in Sec. III.D. As described there, if the original optimal parameters do not pass the validation, additional inflation of $\sigma_{pr_{gnd}}$ and P values are required. However, it is theoretically possible that all constraints would not be satisfied even with the maximum broadcast values of $\sigma_{pr_{gnd}}$ and P value specified in [27], which are 5.08 m and 0.001275 m/m, respectively. If this happens, we can switch to the backup inflated σ_{vig} value described above. An alternative in this case (because the LPs

Table 5 Percentage of approved subset geometries after geometry screening

		Without inflation	σ_{vig} inflation	Targeted inflation
Newark	$c = 1.0$	95.1%	83.2%	86.6%
	$c = 0.5$	95.1%	90.9%	90.5%
Memphis	$c = 1.0$	95.4%	81.7%	86.2%
	$c = 0.5$	95.4%	91.1%	90.3%

were solvable before validation and adjustment) would be to increase the nominal σ_{vig} value in steps of 0.1 mm/km (the minimum increment specified in [27]) until all constraints are satisfied.

The targeted inflation algorithm tries to minimize VPL inflation of the all-in-view geometry, but it does not explicitly optimize VPLs of other subset geometries because these subset geometries have much less impact on system availability. Nevertheless, it is informative to compare how many subset geometries are approved before and after geometry screening using the two different inflation algorithms. Table 5 shows the percentage of approved subset geometries at the two airports and two different c factors examined. All subset geometries over 1440 epochs (1 min updates over a 24 hr period) are evaluated. Geometry screening reduces the percentage of approved subset geometries by up to 13.7 percentage points compared with the preinflation cases. When $c = 1.0$, targeted inflation approves 3–5 percentage points more subset geometries than σ_{vig} inflation does. When $c = 0.5$, σ_{vig} inflation approves about 1 percentage point more subset geometries than targeted inflation does. These differences are fairly small. Although targeted inflation appears to outperform σ_{vig} inflation by this measure, the difference is not likely to affect system performance measurably. (Note that the total number of approved subset geometries is not a critical performance metric because subset geometries other than the all-in-view geometry are used for less than 5% of the time during an airplane's precision approach. Minimization of the VPL inflations of all-in-view geometries is paramount to improve the system availability.)

V. Conclusions

Anomalous ionospheric gradients have become the biggest single concern for single-frequency GBAS operations. To meet system safety requirements in the presence of worst-case anomalous ionospheric gradients without modifying existing category I GBAS avionics and communication protocols, position-domain geometry-screening methods have been previously proposed and implemented. Although the system safety is protected, availability is inevitably reduced by the need to inflate one or more broadcast integrity parameters above the values that would otherwise be required. Existing methods that only inflate the single broadcast σ_{vig} value can result in significant availability loss for category I precision approach operations.

To minimize the availability impact of geometry screening, this paper develops an inflation algorithm called targeted inflation, which inflates the satellite-specific broadcast parameters $\sigma_{pr_{gnd}}$ and P values by a unique optimization procedure. The purpose is to minimize the increase in the all-in-view VPL, which impacts availability the most, while screening out all unsafe subset geometries as required to protect integrity. To make the underlying nonlinear optimization problem feasible in real time, it is simplified into two suboptimal but independent linear programming problems. This targeted inflation algorithm demonstrates clear availability improvements at both Newark Liberty International Airport and Memphis International Airport. Furthermore, the larger margin between inflated VPLs and VAL resulting from this algorithm provides margin against temporary GPS or GBAS system weaknesses and improves system continuity.

Acknowledgments

The authors gratefully acknowledge the Federal Aviation Administration (CRDA 08-G-007) for supporting this research. Jiwon Seo and Sigrid Close acknowledge the support of the National Science Foundation (AGS 1025262-002) and the Office of Naval Research (N00014-10-1-0450). Jiyun Lee was supported by Basic Science Research Program through the National Research Foundation of Korea, funded by the Ministry of Education, Science and Technology (N01100512). The opinions discussed here are those of the authors and do not necessarily represent those of the Federal Aviation Administration or other affiliated agencies.

References

[1] Misra, P., and Enge, P., *Global Positioning System: Signals, Measurement, and Performance*, 2nd ed., Ganga-Jamuna, Lincoln, MA, 2006.

[2] Kaplan, E. D., and Hegarty, C. J. (eds.), *Understanding GPS: Principles and Applications*, 2nd ed., Artech House, Norwood, MA, 2006.

[3] Enge, P., "Local Area Augmentation of GPS for the Precision Approach of Aircraft," *Proceedings of the IEEE*, Vol. 87, No. 1, Jan. 1999, pp. 111–132. doi:10.1109/5.736345

[4] Murphy, T., and Imrich, T., "Implementation and Operational Use of Ground-Based Augmentation Systems (GBASs)—A Component of the Future Air Traffic Management System," *Proceedings of the IEEE*, Vol. 96, No. 12, Dec. 2008, pp. 1936–1957. doi:10.1109/JPROC.2008.2006101

[5] Rife, J., and Phelts, R. E., "Formulation of a Time-Varying Maximum Allowable Error for Ground-Based Augmentation Systems," *IEEE Transactions on Aerospace and Electronic Systems*, Vol. 44, No. 2, April 2008, pp. 548–560. doi:10.1109/TAES.2008.4560206

[6] "Minimum Operational Performance Standards for GPS Local Area Augmentation System Airborne Equipment", RTCA SC-159 DO-253C, 16 Dec. 2008.

[7] Stankov, S. M., Warnant, R., and Stegen, K., "Trans-Ionospheric GPS Signal Delay Gradients Observed Over Mid-Latitude Europe During the Geomagnetic Storms of October–November 2003," *Advances in Space Research*, Vol. 43, No. 9, May. 2009, pp. 1314–1324. doi:10.1016/j.asr.2008.12.012

[8] Moore, R. C., and Morton, Y. T., "Magneto-Ionic Polarization and GPS Signal Propagation Through the Ionosphere," *Radio Science*, Vol. 46, Feb. 2011, RS1008. doi:10.1029/2010RS004380

[9] Datta-Barua, S., Walter, T., Blanch, J., and Enge, P., "Bounding Higher-Order Ionospheric Errors for the Dual-Frequency GPS User," *Radio Science*, Vol. 43, Oct. 2008, RS5010. doi:10.1029/2007RS003772

[10] Morton, Y. T., Zhou, Q., and van Graas, F., "Assessment of Second-Order Ionosphere Error in GPS Range Observables Using Arecibo Incoherent Scatter Radar Measurements," *Radio Science*, Vol. 44, Jan. 2009, RS1002. doi: 10.1029/2008RS003888

[11] Seo, J., Walter, T., and Enge, P., "Availability Impact on GPS Aviation Due to Strong Ionospheric Scintillation," *IEEE Transactions on Aerospace and Electronic Systems*, Vol. 47, No. 3, July 2011, pp. 1963–1973. doi:10.1109/TAES.2011.5937276

[12] Tancredi, U., Renga, A., and Grassi, M., "Ionospheric Path Delay Models for Spaceborne GPS Receivers Flying in Formation with Large Baselines," *Advances in Space Research*, Vol. 48, No. 3, Aug. 2011, pp. 507–520. doi:10.1016/j.asr.2011.03.041

[13] Datta-Barua, S., Walter, T., Pullen, S., Luo, M., Blanch, J., and Enge, P., "Using WAAS Ionospheric Data to Estimate LAAS Short Baseline Gradients," *Proceedings of the 2002 National Technical Meeting of The Institute of Navigation*, Institute of Navigation, Manassas, VA, Jan. 2002, pp. 523–530.

[14] Datta-Barua, S., Lee, J., Pullen, S., Luo, M., Ene, A., Qiu, D., et al., "Ionospheric Threat Parameterization for Local Area Global-Positioning-System-Based Aircraft Landing Systems," *Journal of Aircraft*, Vol. 47, No. 4, July 2010, pp. 1141–1151. doi:10.2514/1.46719

[15] Lee, J., Pullen, S., Datta-Barua, S., and Enge, P., "Assessment of Ionosphere Spatial Decorrelation for Global Positioning System-Based Aircraft Landing Systems," *Journal of Aircraft*, Vol. 44, No. 5, 2007, pp. 1662–1669. doi:10.2514/1.28199

[16] Simili, D. V., and Pervan, B., "Code-Carrier Divergence Monitoring for the GPS Local Area Augmentation System," *Proceedings of the 2006*

IEEE/ION Position, Location, and Navigation Symposium, Institute of Navigation, Manassas, VA, April 2006, pp. 483–493.
doi:10.1109/PLANS.2006.1650636

[17] Lee, J., Seo, J., Park, Y. S., Pullen, S., and Enge, P., "Ionospheric Threat Mitigation by Geometry Screening in Ground-Based Augmentation Systems," *Journal of Aircraft*, Vol. 48, No. 4, July 2011, pp. 1422–1433.
doi: 10.2514/1.55325

[18] Lee, J., Luo, M., Pullen, S., Park, Y. S., Enge, P., and Brenner, M., "Position-Domain Geometry Screening to Maximize LAAS Availability in the Presence of Ionospheric Anomalies," *Proceedings of the 19th International Technical Meeting of the Satellite Division of The Institute of Navigation*, Institute of Navigation, Manassas, VA, Sept. 2006, pp. 393–408.

[19] Pullen, S., Luo, M., Walter, T., and Enge, P., "Using SBAS to Enhance GBAS User Availability: Results and Extensions to Enhance Air Traffic Management," *Proceedings of the 2nd ENRI International Workshop on ATM/CNS (EIWAC 2010)*, Tokyo, Japan, 10–12 Nov. 2010.

[20] Jensen, D., "SLS-4000 GBAS–The Future Is Near," *7th International GBAS Working Group Meeting (I-GWG-7)*, Rio de Janeiro, Brazil, 9 April 2008.

[21] Ramakrishnan, S., Lee, J., Pullen, S., and Enge, P., "Targeted Ephemeris Decorrelation Parameter Inflation for Improved LAAS Availability During Severe Ionosphere Anomalies," *Proceedings of the 2008 National Technical Meeting of The Institute of Navigation*, Institute of Navigation, Manassas, VA, Jan. 2008, pp. 354–366.

[22] Mayer, C., Belabbas, B., Jakowski, N., Meurer, M., and Dunkel, W., "Ionosphere Threat Space Model Assessment for GBAS," *Proceedings of the 22nd International Technical Meeting of the Satellite Division of The Institute of Navigation*, Institute of Navigation, Manassas, VA, Sept. 2009, pp. 1091–1099.

[23] Murphy, T., Harris, M., Park, Y. S., and Pullen, S., "GBAS Differentially Corrected Positioning Service Ionospheric Anomaly Errors Evaluated in an Operational Context," *Proceedings of the 2010 International Technical Meeting of The Institute of Navigation*, Institute of Navigation, Manassas, VA, Jan. 2010, pp. 394–410.

[24] Park, Y. S., Pullen, S., and Enge, P., "Enabling LAAS Airport Surface Movement: Mitigating the Anomalous Ionospheric Threat," *Proceedings of the 2010 IEEE/ION Position, Location, and Navigation Symposium*, Institute of Navigation, Manassas, VA, May 2010, pp. 667–679.
doi:10.1109/PLANS.2010.5507219

[25] Shively, C. A., and Niles, R., "Safety Concepts for Mitigation of Ionospheric Anomaly Errors in GBAS," *Proceedings of the 2008 National Technical Meeting of The Institute of Navigation*, Institute of Navigation, Manassas, VA, Jan. 2008, pp. 367–381.

[26] van Graas, F., and Zhu, Z., "Tropospheric Delay Threats for the Ground Based Augmentation System," *Proceedings of the 2011 International Technical Meeting of The Institute of Navigation*, Institute of Navigation, Manassas, VA, Jan. 2011, pp. 959–964.

[27] "GNSS-Based Precision Approach Local Area Augmentation System (LAAS) Signal-in-Space Interface Control Document (ICD)", RTCA SC-159 DO-246D, 16 Dec. 2008.

[28] Luenberger, D. G., and Ye, Y., *Linear and Nonlinear Programming*, 3rd ed., Springer, New York, 2008.

[29] Pervan, B., and Gratton, L., "Orbit Ephemeris Monitors for Local Area Differential GPS," *IEEE Transactions on Aerospace and Electronic Systems*, Vol. 41, No. 2, April 2005, pp. 449–460.
doi:10.1109/TAES.2005.1468740

[30] Tang, H., Pullen, S., Enge, P., Gratton, L., Pervan, B., Brenner, M., et al., "Ephemeris Type A Fault Analysis and Mitigation for LAAS," *Proceedings of the 2010 IEEE/ION Position, Location, and Navigation Symposium*, Institute of Navigation, Manassas, VA, May 2010, pp. 654–666.
doi:10.1109/PLANS.2010.5507218

[31] "Minimum Operational Performance Standards for Global Positioning System/Wide Area Augmentation System Airborne Equipment", RTCA SC-159 DO-229D, 13 Dec. 2006.